UNIVERSITY OF CALIFORNIA, MERCED

Transient Absorption and Raman Spectroscopy of Cadmium Selenide/Zinc Selenide Core/Shell Alloy Particles

A thesis in partial satisfaction of the requirements for the degree of

MASTER OF SCIENCE

in

Physics and Chemistry

By

Cory R. Sobotta

Committee in charge:

Professor Anne Myers Kelley, Chair

Professor David F. Kelley, Advisor

Professor Erik Menke

Professor Michael E. Colvin

Copyright Information

Figure 4 appears courtesy of http://www.nd.edu/~pkamat/femto.html.

The thesis of Cory R. Sobotta is approved, and it is acceptable in quality and form for publication on microfilm and electronically:

X _____

X _____

X _____
Advisor

X _____
Chair

University of California, Merced

2012

Table of Contents

List of Figures

Acknowledgements

Support for this project came in multiple forms, and I would like to acknowledge each as they were instrumental in allowing me to complete this work. Financial support from teaching assistant positions in general and organic chemistry, as well as GSR positions funded by a Department of Energy grant, were the primary means of support. These positions allowed me to complete my degree and earn a decent salary whilst doing so and are greatly appreciated.

My thanks also go out to the numerous friends and acquaintances I have met throughout my time at UC Merced who have assisted me in my academic endeavors in one way or another. Special thanks goes to Luke Reed, Chenfei Xu, and Deborah Lair for their friendship and indispensable assistance in learning the graduate coursework at UC Merced, as well as their willingness to listen and critique my presentations and thesis. I would also like to thank Dr. Zhongjie Jiang and Dr. Xichen Cai, the postdocs in my group, for their vital assistance with particle preparation and instrumentation, respectively.

I would also like to thank my advisor Dr. David Kelley for his patient explanations of topics I would otherwise find impossible to understand, as well as Dr. Anne Kelley for her expertise in Raman spectroscopy and advice on ways to make this thesis clearer and scientifically more accurate. Finally I express my gratitude to Dr. Erik Menke and Dr. Michael Colvin for their willingness to be part of my Master's Committee and their scientific insights that made this thesis more complete.

Abstract of Thesis

Transient Absorption and Raman Spectroscopy of Cadmium Selenide/Zinc Selenide Core/Shell Alloy Nanoparticles

By

Cory R. Sobotta

Master of Science in Physics and Chemistry

University of California, Merced, 2012

Professor David F. Kelley, Advisor

The central premise of this thesis surrounds the effects of smoothing out the interface between core and shell of a nanoparticle system on the multi-exciton auger recombination kinetics as measured by transient absorption spectroscopy. Current research suggests smoothing out the interface between core and shell by alloying at high temperature reduces the auger rate [1], the rate at which multiexcitons combine down to a single exciton, and therefore increases the viability of the system for solar energy devices incorporating multiple exciton generation (MEG) technology. Auger recombination is so detrimental to these technologies because it occurs on a timescale of picoseconds, whereas radiative recombination, the primary mechanism for capturing energy in a nanoparticle and reemitting it, occurs on the nanosecond timescale. If multiexcitons were to be created in a nanocrystal sample with no means of controlling auger recombination, the auger mechanism would reduce these excitons down to one, and subsequent cooling of the hot

carrier by phonon release would result in the loss of all of the extra energy that was stored in these excitons. In order to study this phenomenon multiple experimental techniques were performed on the nanoparticle samples, most notably UV-Vis, static fluorescence, Raman and transient absorption spectroscopies. As a result of this research, it is clear that alloying a core/shell particle has little effect on transient absorption kinetics, and that current theory on the subject needs to be reformulated.

The experimental data contained herein is compared with calculations using a FORTRAN program developed by Professor David. F. Kelley, and confirms the process of alloying has little to no effect on auger rates of nanoparticles for this system. The calculations were also able to reproduce the UV-Vis and Raman spectra almost quantitatively if given the correct parameters, increasing confidence in the interpretation of the experimental results. This thesis does not aim to discuss what exactly controls the auger rate in nanoparticle systems, but a few conjectures based on sound observation and rooted in solid theory are presented.

Introduction

Cadmium Selenide (CdSe) and Zinc Selenide (ZnSe) make for an optimal semiconductor pair for nanoparticle studies for a number of reasons. The bandgap of CdSe is 1.74 eV (see Appendix), whereas that of ZnSe is 2.58 eV, and because the band alignment is of Type I for a CdSe/ZnSe core/shell system the electrons (conduction band offset of 0.8 eV for this system) and holes (valence band offset 0.2 eV for this system) are both more or less isolated in the core of the nanoparticle [2]. The smaller offset for the holes in the CdSe/ZnSe core/shell system allows for more feasible separation of charge carriers if incorporated into a device, while still maintaining the high luminescence efficiency and stability of the Type I regime. Isolation of the electrons and holes in the core makes processes that trap electrons at the surface less of an issue when it comes to recombination of an electron-hole pair after absorption of a photon. Another reason this semiconductor pair is useful for studying nanoparticle phenomena is the common ion selenium between the core and shell semiconductors, which decreases the lattice mismatch between the materials and allows for easier and more uniform shell growth on the core particles.

In order to achieve enhanced photocurrent for photovoltaic cells employing nanocrystal technology, a process known as multiple exciton generation (MEG) must be maximized. Because of a reduction in momentum conservation and enhanced interaction between electrons and holes in confined nanocrystals, the excess energy of an electron or hole caused by an exciting photon can produce more than one exciton. MEG in nanocrystals is currently a hot topic in the semiconductor field and has been shown to occur in many different semiconductor quantum dots, including CdSe, PbSe, PbS and Si [3].

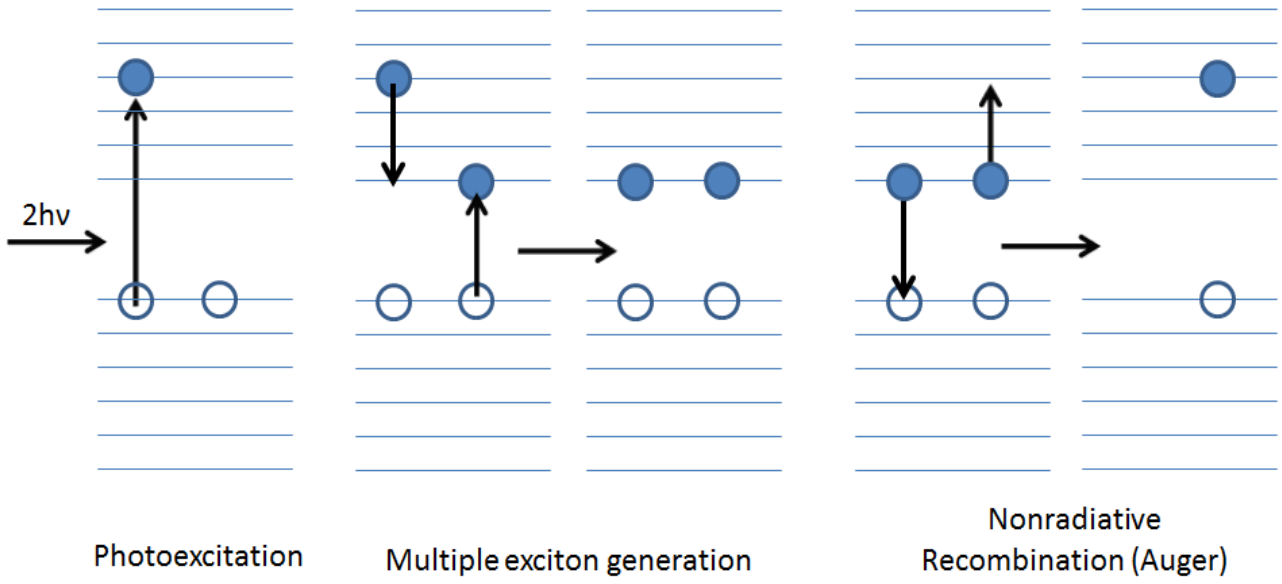

Figure 1: Visual representation of photoexcitation, multiple exciton generation (MEG), and auger recombination as they occur in semiconductor quantum dots. In this case excitation was performed by a photon with energy equal to twice the energy gap of the semiconductor nanocrystal.

In the above diagram, a photon with energy in excess of the energy gap (exactly twice the energy gap) excites an electron from the valence to the conduction band, and the excess energy promotes an additional electron over the energy gap instead of being lost to lattice vibrations, a process known as multiple exciton generation or MEG. MEG can become a faster process than phonon emission in nanoparticles because of the large separation between discrete energy levels in quantum confined systems, a situation known as the "phonon bottleneck" [4]. Auger recombination combines multiple excitons into a single exciton by putting the energy of one exciton into the electron or hole of another exciton, raising it to a higher energy level. Auger recombination occurs on a timescale much faster than radiative recombination (not shown), occurring in picoseconds rather than nanoseconds, respectively.

The process of auger recombination, in which multiple excitons recombine down to a single exciton and release this extra stored energy into molecular or lattice vibrations, also occurs and must be understood in order to maximize MEG. This is quite a serious problem because auger

recombination occurs at a rate that is on the order of a thousand times faster than MEG, and if this process is not controlled it would render solar technology based on nanoparticle MEG no better than current technologies. This is the case because traditionally all of the energy of an excitation photon in excess of the energy gap in a semiconductor solar cell is lost to heat, whereas MEG could result in that energy producing additional charge carriers that would enhance the current, and therefore energy production, generated by these devices. It is the relationship between auger recombination and its detrimental effect on harvesting additional energy from MEG that motivates this project.

As was previously mentioned, mechanisms for reducing the auger rate of nanoparticle systems need to be understood if solar technology utilizing MEG will ever come to fruition. It is currently proposed in the literature that smoothing of the interface between core and shell of a nanoparticle system can reduce the auger rate by 3 orders of magnitude or more by reducing the high spatial frequency components of the ground state wave function [1].

Core/shell particles have undefined slopes in their potential energy functions at the boundary between core and shell which produces uncertainty in momentum of electrons and holes, leading to high frequency components in the wavefunction and supposedly faster auger rates. Alloyed nanoparticles eliminate these components and therefore reduce the auger rate. Cragg and Efros describe the nonradiative auger recombination rate using the following formula that follows from Fermi's Golden Rule [1].

$$\frac{1}{\tau_A} = \frac{2\pi}{\hbar}\int \left|M_{if}\right|^2 \delta\left(E_i - E_f\right) d\mathcal{R}_f$$

Where $\tau_A$is the auger lifetime, M_{if} is the matrix element that describes the Coulomb interaction of the particles (electron and hole), E_i and E_f are the initial and final energies of the

system, and $\mathcal{R}_f$ is the set of variables that completely describe the final state of the system. The authors state that from a Fourier expansion of the ground state, the major component of M_{if} comes from the spatial frequency component k_F, which matches the momentum of excited state electron or holes, and is usually large in systems that have abrupt interfaces [1]. High values of k_F lead to larger values of the matrix element M_{if}, which increases the value $\frac{1}{\tau_A}$, which is the auger recombination rate. This is the theory this thesis sets out to confirm or disprove, and more will be discussed about it later.

In addition to considering the auger and MEG rates for nanoparticle systems other rates come into play when applying this technology to future solar energy devices.

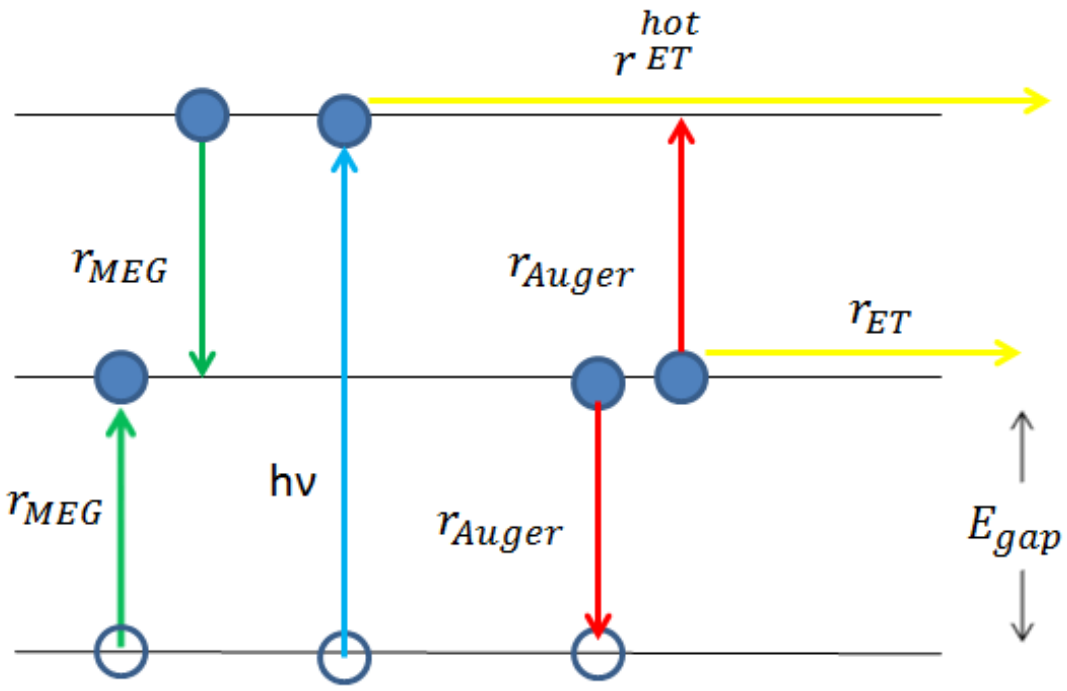

Figure 2: Schematic of the rates involved in a nanoparticle system with regards to their use in solar energy technology. In the figure E_{gap} is the energy gap between the conduction and valence bands of the semiconductor, r_{MEG} is the rate of multiple exciton generation, and r_{ET} is the electron transfer rate away from the nanocrystal.

Following the above diagram, multiple exciton generation (MEG) must be faster than auger recombination and the rate at which electrons leave the nanoparticle or activate phonons and cool, and electron transfer must be faster than auger recombination and standard radiative recombination [4]. The rate of MEG must also be faster than hot electron transfer and cooling of electrons through phonon activation. Electron transfer from the nanoparticle must be faster than radiative recombination or the extra electrons produced through MEG will be lost, and finally electron transfer must be faster than auger recombination [6]. If all of these rates are carefully controlled it may be possible to harness multiexcitons to produce more efficient solar energy devices.

In addition to the above rates surrounding multiexcitons, there are other processes to consider that can lead to the loss of charge upon photoexcitation of a nanocrystal. In addition to surface trap sites, charge carriers may be neutralized by redox species in solution [2], or get trapped in a defect site in matrices if the particles are in a solid-state sort of device. With this daunting set of rates and processes to consider it comes as no surprise that devices utilizing nanoparticle technology are not currently available. With what seems like a world full of factors against this sort of technology being possible in the near future, a review of some current literature on topics relevant to this thesis will motivate the experimental portion of this thesis.

Review of Previous Work

Several literature reports have motivated at least part of this project at varying times during its gestation, and will be discussed here. The literature items on the agenda are a review of composition-tunable alloyed nanocrystals [7], followed by suppression of auger processes in confined structures [1], a paper on non-blinking semiconductor nanocrystals [5], and finally implications of MEG for purposes of solar energy harvesting [4].

Composition-Tunable Alloyed Semiconductor Nanocrystals [7]

The central premise of this body of work and the reason it applies to this thesis is that alloying of two semiconductor materials, such as those that are in a core/shell arrangement, produces properties unique to either of the parent semiconductors alone [7]. These properties manifest themselves when the compositions of the constituent semiconductors have a radial gradient, unlike a traditional core/shell particle which possesses uniform distribution of elements that are separated into core and shell regions.

By controlling the composition of the gradient alloy nanoparticles it is possible to tune the emission of a sample of nanoparticles outside of its traditional spectral window, allowing for another means of "bandgap engineering" not related to the size of the particles. For example, the authors cite the example of CdSe being unable to emit in the near-infrared (800nm+) region of the electromagnetic spectrum. By alloying CdSe with CdTe and forming $CdSe_xTe_{1-x}$, however, the near-infrared emission is attainable at very high efficiencies.

Likewise a few reports have described alloys of CdSe and ZnSe ($Zn_xCd_{1-x}Se$) with the ability to emit in the blue and green regions of the spectrum, a region not normally accessible for either semiconductor by itself. These results are very important because they allow for

optoelectronic and bio-imaging technologies using these nanoparticles to be possible in the near future. Also, being able to tune nanoparticle emission throughout a broader spectral range makes discovering a semiconductor core/shell pair for harnessing solar energy much easier, as it allows for more possibilities that could yield the optimal bandgap.

Suppression of Auger Processes in Confined Structures

This paper is a mathematical analysis of what happens when the potential energy function of a core/shell system is smoothed out by alloying the core/shell nanoparticle. The authors calculate upwards of a thousand times reduction in auger rates in alloyed core/shell particles compared to those with abrupt boundaries; the reduction coming from eliminating the high spatial frequency components of the ground state wavefunction encountered between two different materials [1]. Cragg et al. use the following equation for their auger rate calculations:

$$\frac{1}{\tau_A} = \frac{2\pi}{\hbar}\int |M_{if}|^2 \delta(E_i - E_f) d\mathcal{R}_f$$

Where $\tau_A$is the auger lifetime, M_{if} is the matrix element that describes the Coulomb interaction of the particles (electron and hole), E_i and E_f are the initial and final energies of the system, and $\mathcal{R}_f$ is the set of variables that completely describe the final state of the system. The authors state the major factor causing M_{if} to be large following a Fourier expansion is the spatial frequency component k_F, and large k_F values are obtained from calculations on abrupt potential changes, such as that of the interface between two unlike materials.

The ground state wavefunction for a particle-in-a-box, the model the authors used to describe particles with abrupt interfaces (non-alloyed core/shell particles), is given by:

$$\psi(x) = \sin\left[\frac{\pi\left(1 - \frac{x}{a}\right)}{2}\right] * \frac{1}{\sqrt{a}}$$

Where x is the position inside the box, and a is the half-width of the box. This function has a Fourier transform proportional to $1/(k_F a)^2$.

Contrast this with a parabolic profile, or the profile created by an alloyed nanoparticle.

The ground state wavefunction for a parabolic potential is given by:

$$\psi(x) = \exp\left(-\frac{x^2}{2a^2}\right)/(\sqrt{\pi a})^{1/2}$$

Which has a Fourier transform proportional to $\exp(-\frac{k_F^2 a^2}{2})$. It turns out when k_F is much larger than 1/a, the Fourier component corresponding to the abrupt box potential is exponentially larger than that associated with a smooth, parabolic profile [1]. This is mainly due to the negative exponent in the parabolic profile case, which leads the authors to suggest annealing of an abrupt interface into a smooth one as a method to dramatically reduce auger rates. No experimental evidence to reinforce the authors' calculations was given in this body of work.

Non-blinking Semiconductor Nanocrystals

An interesting phenomenon in nanoparticle science is the tendency of nanocrystals of most (if not all) materials to photoluminesce intermittently, even if the sample is constantly under excitation [5]. The authors of this work have developed a radially-graded CdZnSe/ZnSe alloy which no longer exhibits blinking behavior, a significant discovery if one is interested in applications requiring the continuous output of photons, such as nanocrystals as biological labeling devices [5]. The consensus among researchers is that blinking behavior is caused by extra charges in a nanocrystal that increase the rate of auger processes, a situation which would drastically decrease the usefulness of this technology in solar energy devices.

In this experiment the authors compared the photoluminescence behavior of the non-blinking ZnCdSe/ZnSe alloyed particles with that of CdSe/ZnSe crystals, and found the latter, being a typical core/shell system, displayed traditional blinking behavior. Photoluminescence was measured on the timescale of hours so this eliminates any chance the data was an anomalous occurrence over a short period of time. The significance of this project can be seen in potential applications of nanoparticles as single-molecule biological labeling devices and lasers.

Mechanisms for Photogeneration and Recombination of Multiexcitons in Semiconductor Nanocrystals: Implications for Lasing and Solar Energy Conversion

This article is important as it describes the advantages to utilizing nanoparticles in solar energy devices, as well as some present theories on how multiple exciton generation and recombination take place [4]. Many theories on the mechanism for MEG are discussed, and because the topic is still being debated only a few comments will be discussed here; I would instead like to focus on the solar energy conversion sections of the article as they are directly relevant to this thesis. The author states processes like MEG and auger recombination become highly efficient in nanocrystals due to strong confinement of electronic wave functions and the enhancement of electron-hole interactions at the nanometer scale [4].

One widely known fact about solar cells is the limit to their efficiency, calculated by Shockley and Queisser in 1961 to be approximately 30% for a single-junction solar cell [8]. By utilizing nanoparticle and MEG technology, which uses excess photoexcitation energy to produce more than one electron-hole pair per excitation photon, the maximum conversion efficiency under the sun's radiation for a single junction solar cell increases about 50%. The concept of maximum efficiency also depends on what semiconductor is being used, as some

semiconductors can have as many has 8 excitons at a given time for their lowest level 1S ($1S_h$ to $1S_e$) energy transition.

The authors calculate the theoretical maximum conversion efficiency for a single-junction solar cell utilizing MEG technology, a value that approaches 42%. The ideal nanocrystal for such a device would utilize PbSe with a bandgap of 0.45 eV, as this yields the best balance between power output and MEG capability under the radiant power of the sun [4]. The authors describe an ideal solar cell based on nanocrystal and MEG technology in the following manner.

The ideal solar cell described by this work includes n and p electrodes that are connected by hole and electron-conducting wires. Nanocrystals are placed in contact both with one another and the electron and hole conducting wires. The device would be prevented from short circuiting by the placement of electron and hole-blocking layers at the p and n electrodes, respectively. The final component of the solar cell is the external resistor connecting the n and p electrodes. This fictitious solar cell provides the schematic for which the calculations on efficiency (discussed earlier) were based.

The current work provides a method for easily determining the interface sharpness between core and shell in a nanoparticle system, and will attempt to establish whether or not alloying of a core/shell interface in a sample of nanocrystals decreases the auger rate. Experimental visible spectroscopy data will be modeled to help determine sizes of nanoparticles without the need for costly and time-intensive imaging techniques, and Raman results will be reinforced by calculations using the same program. Experimental details regarding the synthesis of the core, core/shell and core/shell alloy nanoparticles are shown below.

Experimental

All syntheses were done using airless techniques in a nitrogen atmosphere on a Schlenk line.

2.1 Reagents

Methanol and hexanes were purchased from Fisher and were of the highest purity available. Se powder, ZnO and chloroform were purchased from Alfa Aesar and were of the highest purity available. Oleic acid (tech., 90%) and Zn Stearate (ZnStearate, ZnO 12.5-14%) were also purchased from Alfa Aesar. Toluene (>=99.3%), octadecene (tech., 90%), octadecyl amine (tech., 90%), cyclohexane (HPLC, 99.9%), and trioctylphosphine oxide (tech., 90%) were all purchased from Aldrich. Trioctylphosphine oxide (TOPO) was additionally purified by recrystallization with acetonitrile.

2.2 CdSe core synthesis

Synthesis of the CdSe core nanospheres was performed using a modified version of the procedure pioneered by Peng et al. [9]. A typical synthesis involves heating 0.0265g (0.2mmol) CdO, 0.252 mL (0.8mmol) oleic acid and 2.55 mL (2g) ODE (octadecene) to 200 C to make a transparent solution. The solution is then cooled to room temperature and 1.5g ODA (octadecyl amine) and 0.5g TOPO (trioctyl phosphine oxide) are added. This solution is heated to 280 C and a solution of 2mmol of Se, 0.472g TBP (tributyl phosphine) and 1.37g ODE is quickly injected. The spheres are grown at 250 C, and the size of the resultant nanospheres is determined by the reaction time. Thirty seconds of reaction time, followed by rapid cooling using a hairdryer set to cool mode (temperature drops from 250 to 125 C in one minute) consistently produces spheres with a diameter of roughly 3.8 nm, the size used for all experiments in this thesis. This size is based on UV-Vis spectra taken after the synthesis and based on imagine studies performed by Peng et al [10].

2.3 CdSe/ZnSe core/shell synthesis

Before synthesis of the core/shell systems, the CdSe cores were extracted with chloroform/methanol to remove any excess precursors. In order to grow a thin shell on the nanospheres a low reactivity ZnOleate precursor was used. The precursor was made following a method from the literature [11]. Typically, a mixture of 0.26g ZnO and 2.54mL oleic acid is heated to 350 C, cooled to room temperature and mixed with 2 mL of TOP (trioctyl phosphine). Separately, 0.2528g Se and 5.8mL TOP are mixed together then added in with the ZnOleate precursor; the combined precursor mixture is non-turbid and added to a solution of the nanospheres in ODE/ODA at 195 C for shelling. Typically the shelling process was run for roughly 3 hours in order to give the precursors enough time to react with one another on the surface of the nanoparticles.

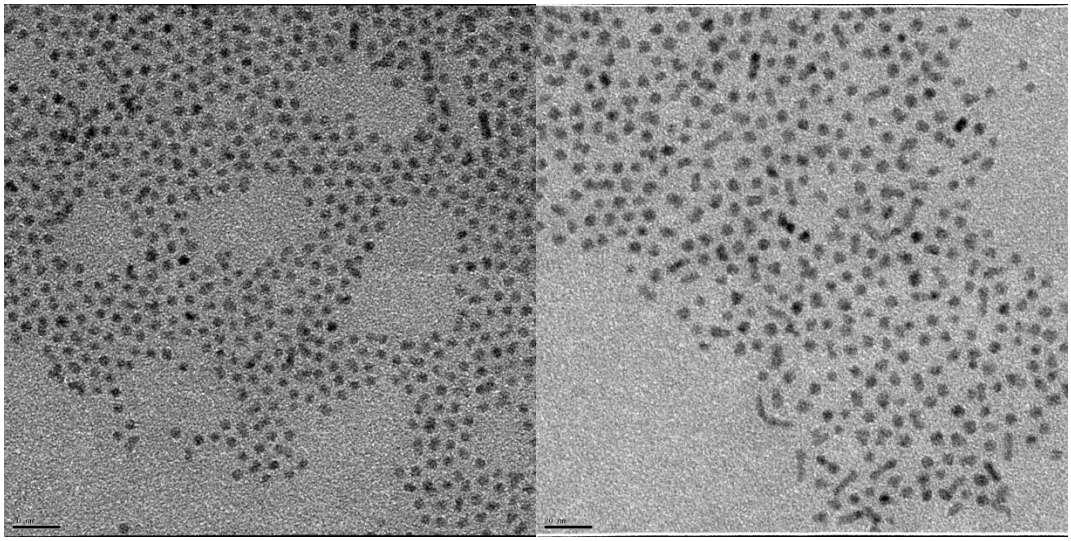

Figure 3: TEM images of CdSe core particles (left) and CdSe/ZnSe core/shell particles (right). The scale bar is 20nm in both images and their average diameters are 3.69nm with a standard deviation of 0.21nm for the cores, and 4.67nm with a standard deviation of 0.30nm for the core/shells.

2.4 CdSe/ZnSe core/shell alloys

CdSe/ZnSe core/shell alloys were prepared by heating a solution of the purified core/shell particles at 250 C for approximately 4 hours under nitrogen, with aliquots taken every hour. UV-Vis, static fluorescence and transient absorption spectroscopies were performed on these as well as the shelling samples collected before alloying.

2.5 Raman Instrumentation

Raman spectra of core, core/shell and alloyed core/shell particles were taken with samples in 1mm cuvettes. Spectra were taken using a Coherent Innova 90C-5 argon-ion laser in continuous wave mode utilizing a Jobin-Yvon T64000 Raman microscope. The microscope has a 0.64m triple spectrograph connected to a confocal Raman microprobe based on an Olympus BX-41 microscope with a 10X objective. The detector is a back-illuminated, UV-coated liquid nitrogen cooled CCD with a quantum efficiency of 50% in the 220 to 850 nm spectral range. The primary wavelength used was 457.9nm, for which the instrument has a spectral resolution better than 4 cm^{-1}. Excitation power at the sample was between 4.5 to 5.5 mW for all samples tested.

2.6 Transient absorption instrumentation

Transient absorption spectra were taken on a custom instrument resembling the following diagram, with a few minor exceptions. The instrument consists of a Clark CPA 2001 light source and Princeton Instruments liquid nitrogen cooled CCD. The light source puts out 150 fs pulses, 600 μJ, 775 nm at a repetition rate of 1 kHz. The sample is excited with a wavelength of 387.5nm. Excitation power at the sample was around 7 mW, and is focusing on an area of about 1 mm^2. All samples were stirred rapidly in 1 cm spectroscopy cuvettes, and had an absorption at 387.5nm of approximately 1.5. The extinction coefficient of the nanospheres at the excitation wavelength was 2.1 x 10^5 L $mol^{-1}cm^{-1}$.

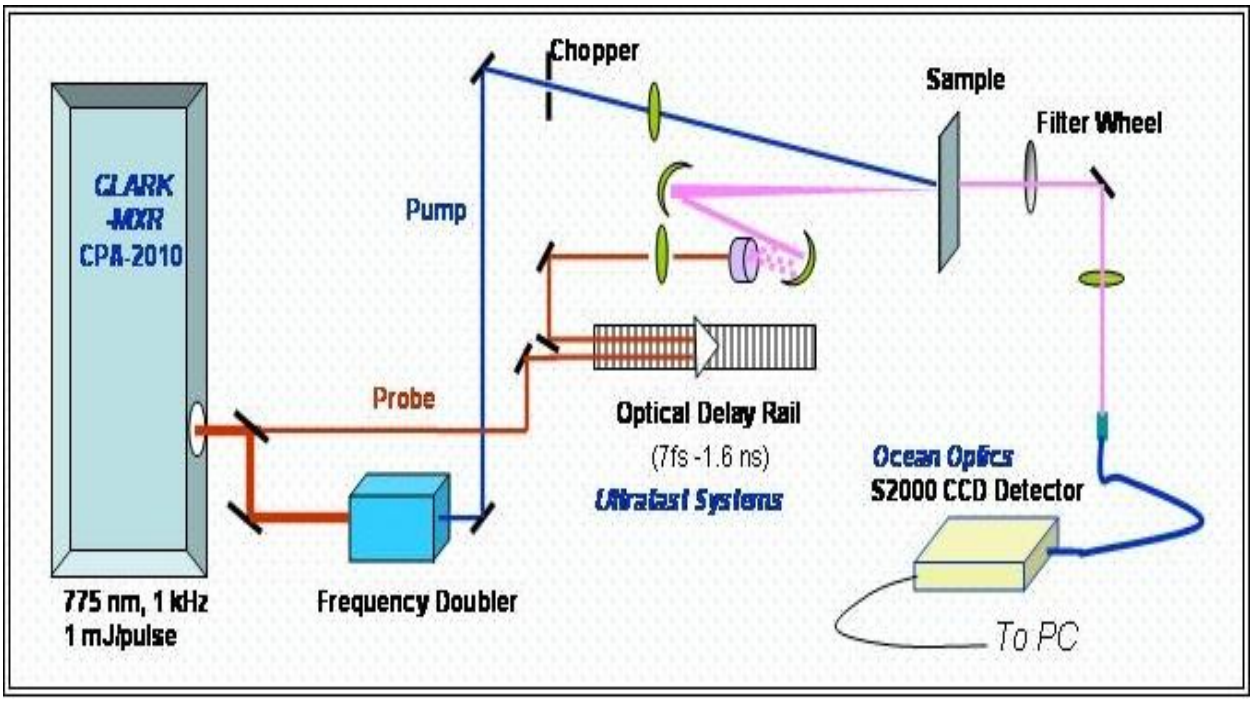

Figure 4: Transient absorption apparatus setup. This work utilized a Clark-MXR CPA-2001 laser, and Clark-MXR brand OPA (optical parametric amplifier). Data is collected instead on a Roper-Scientific brand CCD. The remainder of the setup is very similar to this diagram. This figure comes from http://www.nd.edu/~pkamat/femto.html.

Results and Discussion

The motivation for this project stems from the desire to create more efficient solar energy technologies using multiple exciton generation, or MEG. In order to determine how effective MEG could possibly be in future technologies one must analyze the reverse process, auger recombination, in an effort to learn how to control it. The following experimental data and subsequent discussions will shed some light on what does and does not affect the auger rate in CdSe core, CdSe/ZnSe core/shell, and CdSe/ZnSe core/shell alloy nanoparticles.

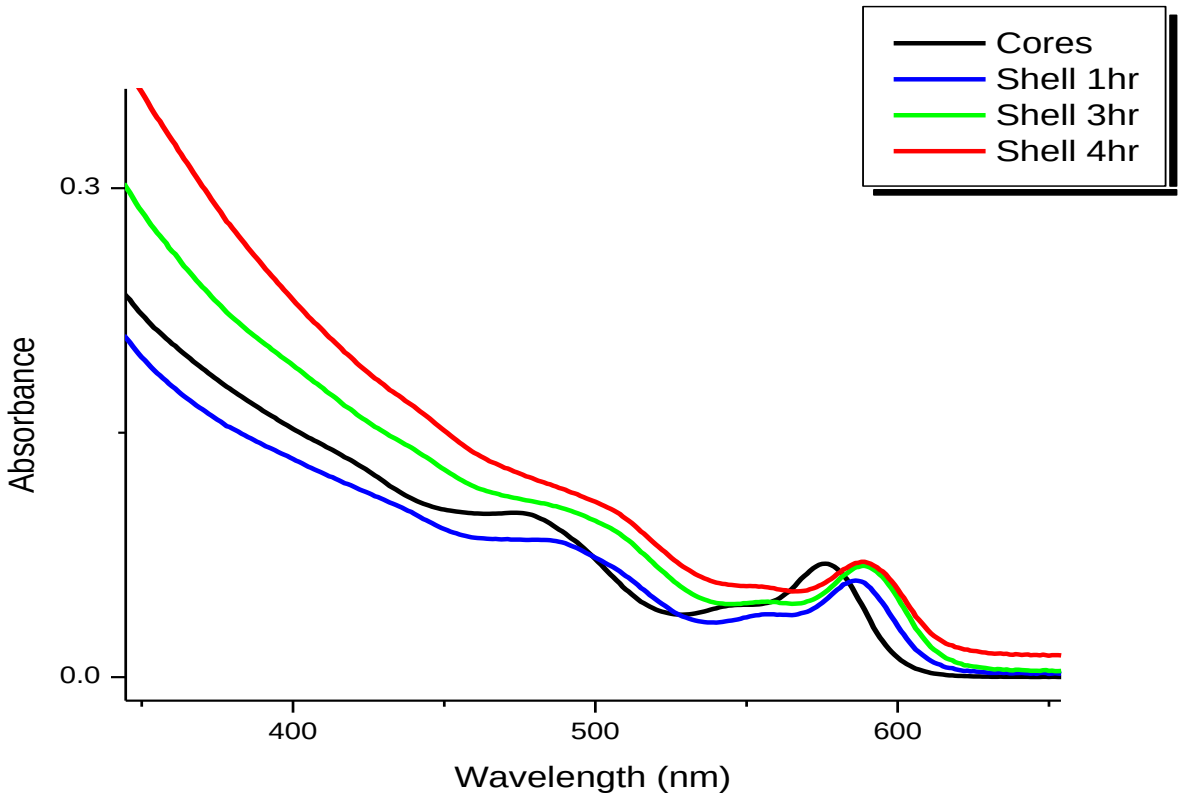

Figure 5: UV-Absorption spectra of core and subsequently shelled particles. Shell 1hr, Shell 3hr and Shell 4hr were taking during the reaction and represent growing a shell of ZnSe on top of the CdSe cores. The redshift in absorbance as shelling progresses can be understood with the particle in a box model, with the box in this case being a sphere.

Quantum confinement decreases as the particle size increases, (the shell growth physically increases the size of the system) which results in a smaller difference between the conduction and valence band energies of the core/shell system, causing the absorbance to redshift to longer wavelengths (lower energies). The CdSe cores have a first excitonic absorption maximum at 576nm, and subsequent shelling redshifts this number to 588nm. It is clear from the UV-Vis spectra above that ZnSe was formed on the surface of the particles due to a drastic absorbance increase starting at 500nm and extending to higher energies (the bandgap of ZnSe is such that it absorbs at 480nm and below). This is corroborated by the fact that the emission spectra below show no sign of ZnSe emission and the Raman spectra below show evidence of ZnSe formation, forcing us to conclude that all ZnSe present is in the form of a shell on the CdSe core particles. The shell of ZnSe is approximately 0.30nm in thickness, and was determined by TEM measurements (see experimental section).

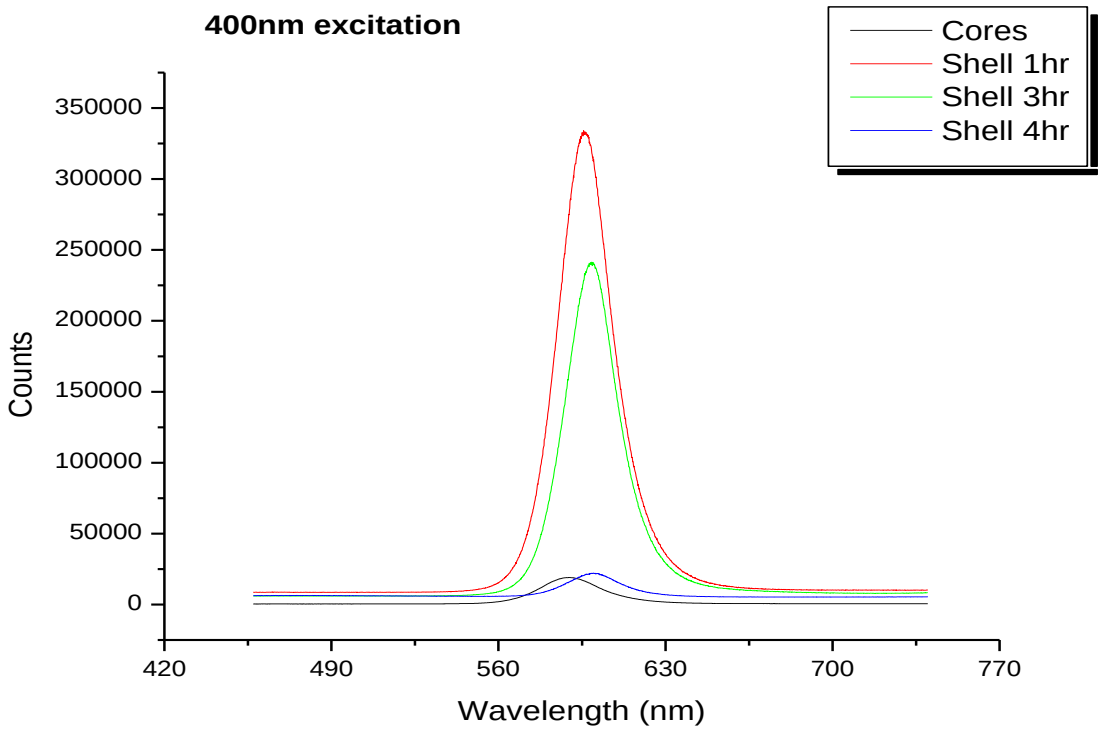

Figure 6: The emission spectra discussed above, for core and core/shell particles excited with 400nm light. Notice the lack of emission anywhere but the major peak around 600nm, indicating the presence of only core/shell particles. If ZnSe were present in solution (and not on the particles) an emission around 500nm would be observed.

Another insight gained from the emission spectra is the increase in luminescence from the cores to shell 1hr and shell 3hr, caused by passivation of surface defects on the core particles. If more shell precursor is added the luminescence begins to greatly diminish again, most probably due to defects in the ZnSe shell caused by stacking faults. This intricacy can be seen throughout all core/shell syntheses and motivates the next portion of the experiment, alloying of the core/shell particles to reduce these stacking faults, and testing the effect of interface sharpness on auger rates.

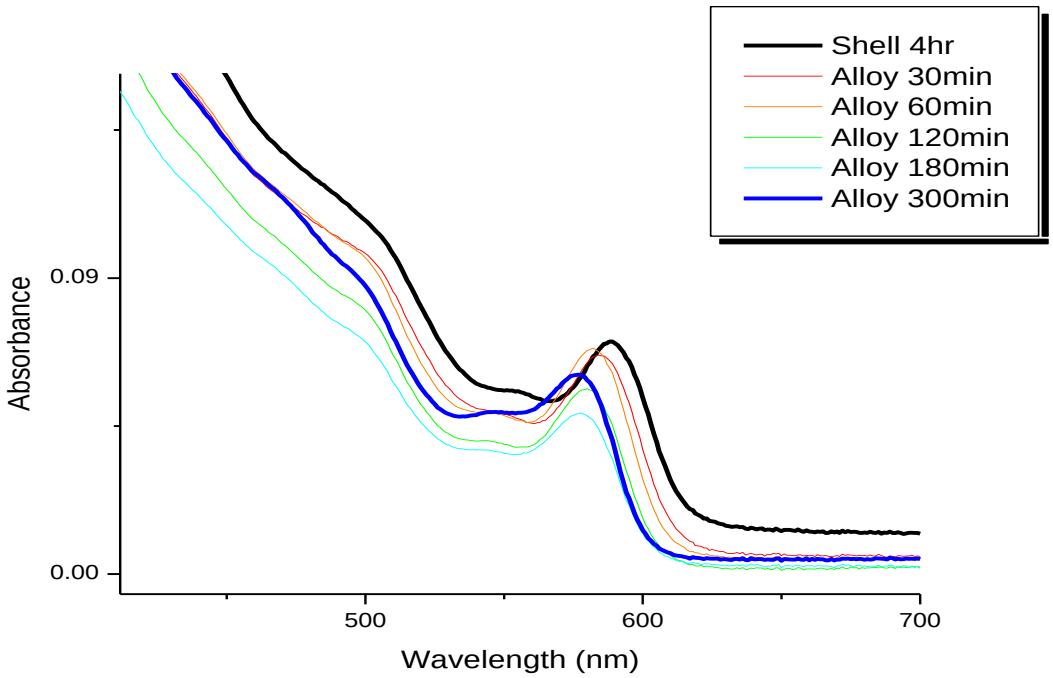

Figure 7: UV-absorption spectrum of the core/shells from the previous figure, along with the spectra obtained when these same particles are alloyed (heated at 250 C) for 30, 60, 120, 180, and 300 minutes.

Notice the reversal of the redshift seen in the core/shell sample, as the core/shells are alloyed they begin to blueshift to higher energies. The blueshift can be explained using the same particle in a sphere model as before, however the first exciton absorption peak increases in energy because of diffusion of the ZnSe shell material into the CdSe core. Diffusion into the core of the particle effectively reduces the size of the core, increasing quantum confinement and therefore the excitonic energy. The core/shells without alloying have a first excitonic absorption maximum at 588nm, and the alloys absorb at 585, 582, 580, 577, and 576.5nm (from shortest to longest alloying time). The magnitude of the blueshift is rather large at about 12 nm, comparable to the redshift obtained when the core particles have shells placed on them.

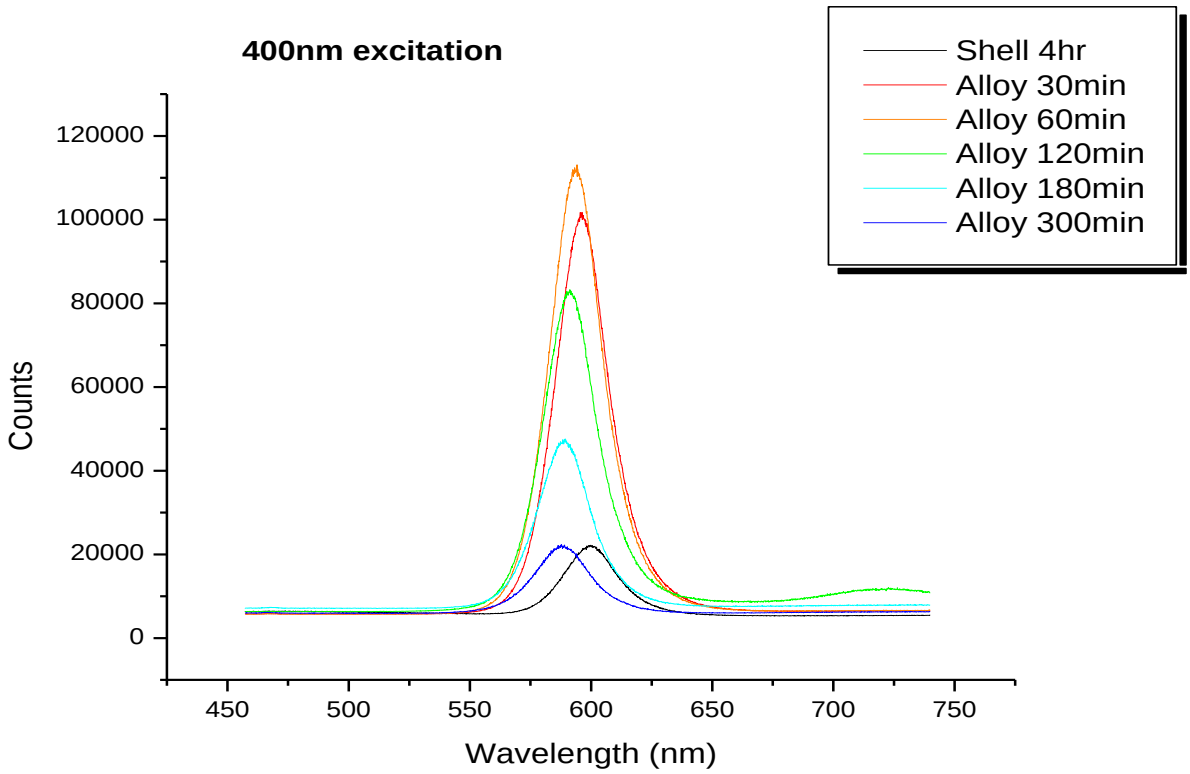

Figure 8: Static fluorescence of alloyed CdSe/ZnSe core/shell particles excited with 400nm light. The intensity of fluorescence increases dramatically at the beginning of alloying up until the first hour, and after five hours the florescence is comparable to the core/shells before alloying.

The dramatic increase in fluorescence for the first hour of alloying can be understood by the annealing out and therefore reduction of any defects present, whether they are surface traps or stacking faults caused by the difference in the lattice spacings of the two materials (see Appendix for lattice mismatches of CdSe/ZnSe). Generally after more than a layer or so of shell material is placed on the particle the fluorescence begins to decrease as the shell material is not placed on properly, but this depends on how disparate the lattice spacings of the core and shell material are. After having an understanding of the absorption and emission spectra the next course of business was to determine the sharpness of the alloyed core/shell interface, and this is where Raman spectroscopy came into play.

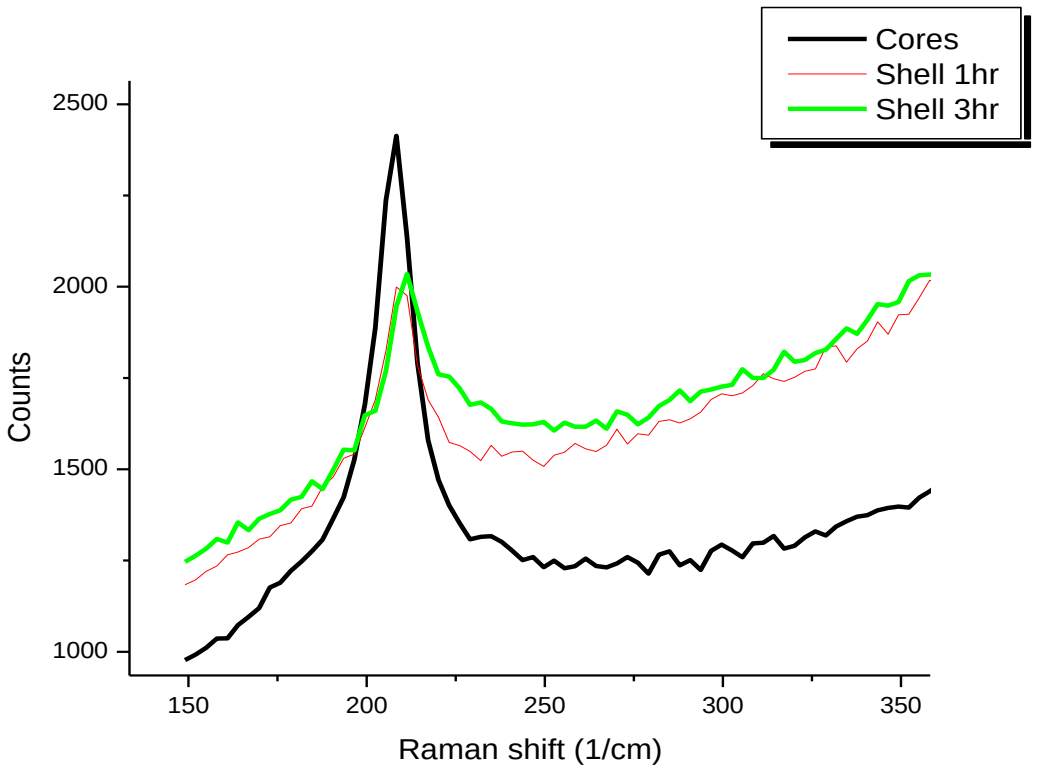

Figure 9: Raman spectra of CdSe core and CdSe/ZnSe core/shell particles.

Raman spectroscopy can be used to probe the structural differences between nanocrystal samples if the longitudinal optical phonon of the material is known. For CdSe the LO phonon is at approximately 208 cm^{-1}, and is always a sharp peak with sharp slopes on either side. The Raman spectra of the core/shell particles show significant broadening on the higher wavenumber side of the CdSe LO phonon along with a small shift to higher wavenumbers, which is indicative of ZnSe growth (the ZnSe LO phonon is at approximately 250 cm^{-1}. If this is taken into account with the UV and fluorescence data it is very clear that ZnSe has formed a shell on the CdSe core particles. Nucleation of ZnSe in solution during preparation of the core/shell particles would result in two emission peaks and a drastically different Raman spectrum, both of which are not seen in experimental data.

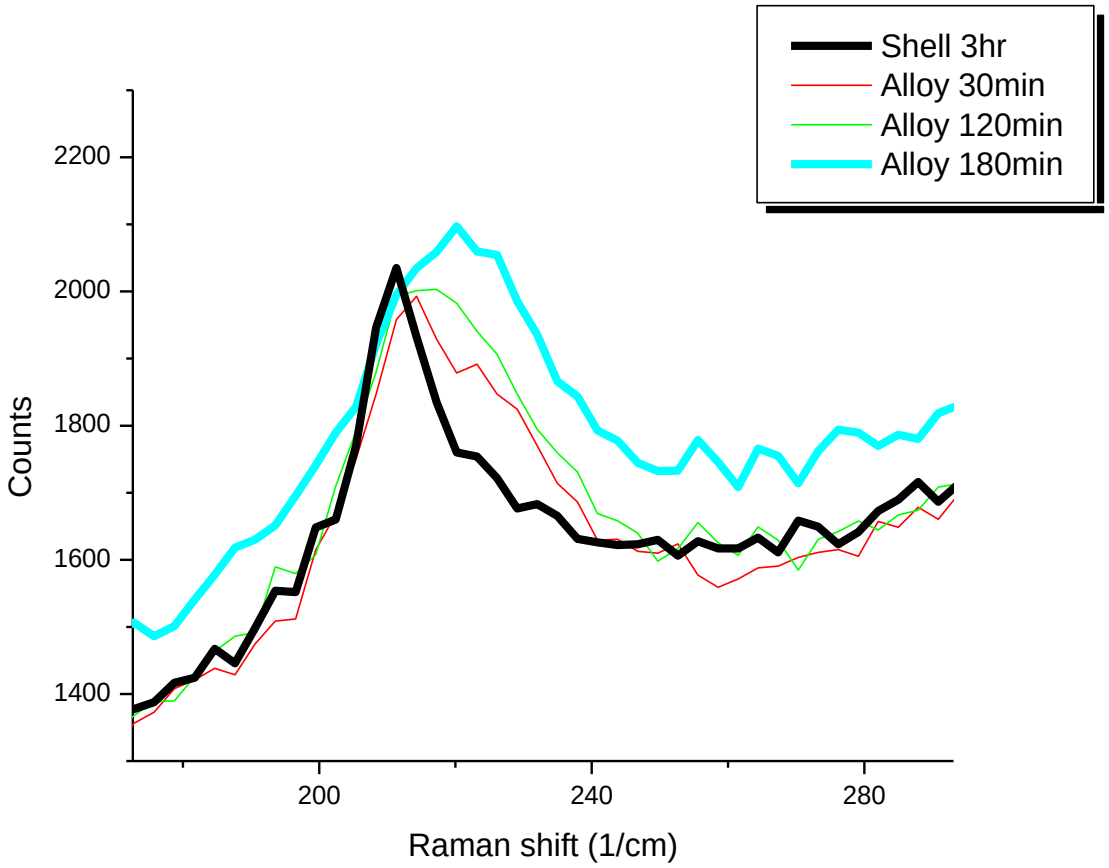

Figure 10: Raman spectra of alloyed CdSe/ZnSe core/shell particles. Comparing the Shell 3hr sample to the alloyed samples it is clear that a drastic change in the LO phonon has taken place. As alloying occurs the LO phonon for CdSe shifts dramatically to higher wavenumbers and broadens considerably.

Consider the shell material diffusing into the core of the nanoparticle, and it becomes clear why the CdSe LO phonon shifts closer to that of the LO phonon of ZnSe. Because vibrations in a crystal are related to the strength and rigidity of the bonds between atoms in the crystal, diffusion of shell material into the core creates a hybrid CdZnSe structure which must have a higher phonon frequency than CdSe but lower than ZnSe. The Raman spectra of the core/shell particles display a slight shift of the CdSe LO phonon toward higher wavenumbers, which could be due to a small amount of alloying taking place during shelling, or compressional

effects caused by the shell material. This effect can also be seen in the UV-Vis spectra, where calculations predict the shelled particles to redshift in absorption to 592nm, but experimentally they only reach 588nm.

Comparison to Calculations

In order to model the experimental spectra a FORTRAN program was written by Professor David Kelley and is used here with permission. The program uses the following parameters in its calculations: it assumes a core radius of 1.85 nm, a thin-shell thickness of 0.25 nm (about one layer of ZnSe), a conduction band offset of 0.8 eV, a valence band offset of 0.2 eV, and assumes the electron and hole are localized inside the particle. The band offsets are such that the CdSe/ZnSe particles are treated as Type I, although the valence bands of CdSe and ZnSe differ only slightly from one another. Other values used are core and shell electron effective masses of 0.11 and 0.22, respectively, and core and shell hole effective masses of 0.44 and 0.60, respectively (these values are for bulk CdSe and ZnSe, see Appendix). One of the major approximations used in this program is that of the localized phonon, or a vibration induced in one small part of the crystal has no effect on the other parts of the crystal.

The program calculates the electron and hole wavefunctions, their interactions and the energies of their overlap, and then does a Fourier-Bessel transform of the lowest electron and hole wavefunctions to give the energy of the lowest energy absorption feature. The program calculates the Raman spectrum for a sample by using its composition to determine where the LO phonon should be. For example, if a sample contained equal amounts of CdSe and ZnSe, it would calculate a Raman frequency halfway between the LO frequencies of pure CdSe and ZnSe. The calculation also takes into account resonance enhancement by determining the product of electron and hole wavefunctions using the local phonon approximation, which may be

a less-than-ideal solution but it yields results that agree rather well with experiment. Another approximation this program contains is that it neglects stress and compression effects induced by placing a shell material with a smaller lattice parameter onto a core particle.

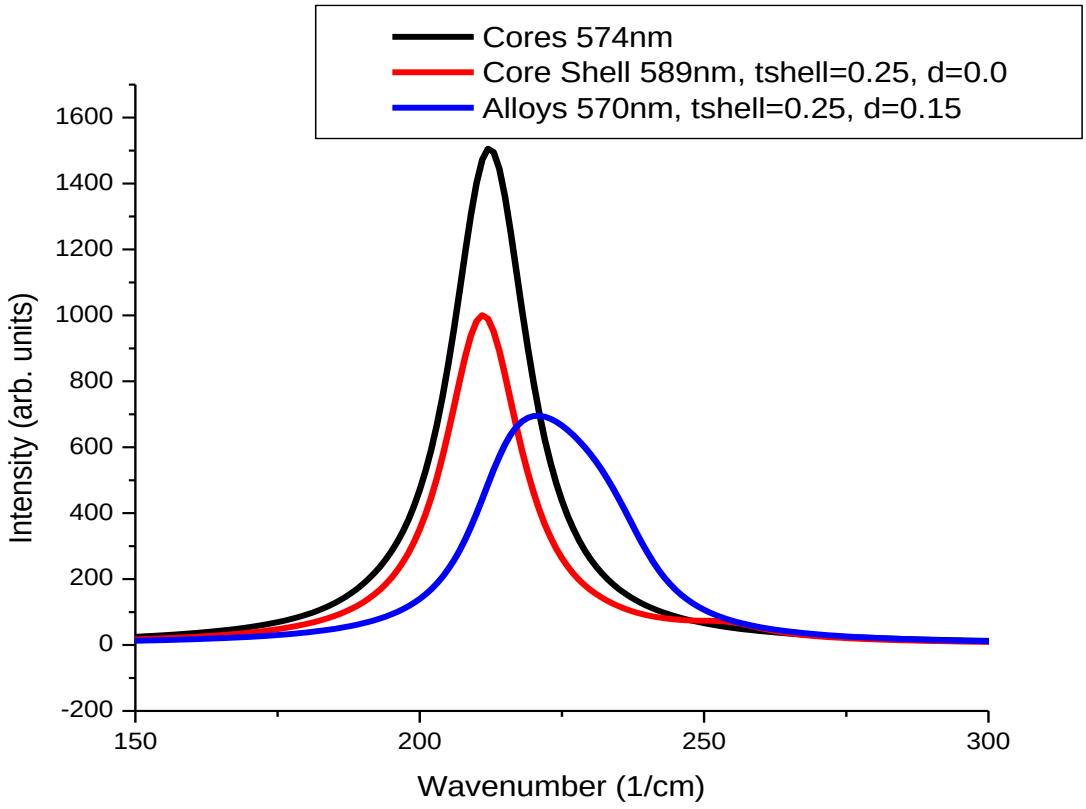

Figure 11: Raman and UV-Vis calculations for a thin-shell case using the program described earlier.

The above figure shows Raman and UV-Vis calculations for a theoretical system, starting with cores that display a first absorption onset of 574nm, which was the experimental value for the above raw data. After a thin shell is placed on the particle surface (0.30nm radially, or equivalent to 1 monolayer of ZnSe) and assuming no diffusion of shell material into the core has occurred, the first absorption onset shifts to 589nm, also in line with experimental values. Finally, if the diffusion parameter is arbitrarily set to D = 0.15, the first absorption onset

blueshifts back to 570 nm. This behavior of redshifting upon shelling and blueshifting upon annealing is seen experimentally in more-or-less equivalent magnitudes.

After depositing a shell of 0.25 nm, or about one layer of ZnSe, the absorption peak shifts to 589 nm, or extremely close to where the experimental particles absorb (588nm). If the diffusion parameter, which determines how much ZnSe diffuses into the CdSe core, is now turned to a value of 0.15, a first absorption onset of 570 nm is obtained (experiment shows 575nm). What this calculation means is diffusion of the shell material into the core causes a blueshift of the absorption, which can be interpreted as the CdSe core getting smaller and therefore more quantum confined. Interestingly enough the Raman spectrum above matches experiment almost quantitatively, diffusion of ZnSe into the CdSe core causes an increase in the Raman wavenumber and a broadening on the higher energy side of the LO phonon peak of CdSe. Broadening of the Raman peak is interpreted as an increase in energy of the phonon caused by a material with lower mass (Zinc) diffusing into a material of higher mass (Cadmium), increasing the energy of their vibrations (phonons) by making them happen more quickly.

The figure above also depicts the calculated behavior of the Raman spectra for the core, core/shell, and core/shell alloy nanoparticles. Application of a ZnSe shell on the CdSe particles slightly shifts the LO phonon frequency to higher wavenumbers (probably due to a small amount of alloying taking place during shelling), whereas alloying drastically shifts the LO phonon frequency of the nanoparticles higher. This behavior and the magnitude of shifting is almost identical to experiment (see earlier figures) and is due to ZnSe from the shell of the nanoparticle diffusing into the nanoparticle core, making the LO phonon frequency of CdSe closer to that of ZnSe (ZnSe has an LO phonon frequency of about 250 cm^{-1}). The fact that almost quantitative agreement between calculations and experiment can be achieved means identifying

characteristics such as degree of alloying and extent of shelling can be understood by simply running a few calculations. Comparing the first excitonic absorption maximum and maximum Raman intensity frequency yields the following results.

Sample	1st Abs. Max. (nm)	Raman peak (cm^{-1})
Shell 1hr	586	210
Shell 3hr	**588**	**211**
Alloy 1hr	582	216
Alloy 3hr	**575**	**220**

Table 1: 1st Absorption maxima and highest intensity Raman peaks for experimental core/shell and core/shell alloy samples.

Calc. parameters	1st Abs. Max. (nm)	Raman peak (cm^{-1})
Tshell = 0.25, D = 0.00	**589**	**211**
Tshell = 0.25, D = 0.15	**570**	**221**

Table 2: 1st Absorption maxima and highest intensity Raman peaks for calculated core/shell (Tshell = 0.25, D = 0.00) and core/shell alloy (Tshell = 0.25, D = 0.15) samples.

As can be seen in the above tables, simulating a CdSe/ZnSe core/shell system with the program results in a first absorption maximum of 589 nm for the core /shell particles, and 570 for the alloyed core/shell particles. These values are in line with the experimental core/shell first absorption maximum of 588nm and alloyed core/shell absorption maximum of 575nm. The agreement between experimental and calculated Raman spectra is even closer, with experiment yielding 211 and 220 cm^{-1} for the core/shell and core/shell alloy respectively, and 211 and 221 cm^{-1} for the calculated core/shell and core/shell alloy. One can also calculate values to compare to the intermediate shelling and alloy samples, but this is unnecessary due to the strong agreement between the initial and final values. Because of almost quantitative agreement

between experimental and calculated UV-Vis and Raman spectra it becomes possible to easily determine the structure and core/shell interface of a nanoparticle system quickly and without the need for expensive, time-consuming equipment.

Below is the composition of the core/shell particles as calculated by the same FORTRAN program, using the same parameters as those that gave the previous Raman and UV spectra.

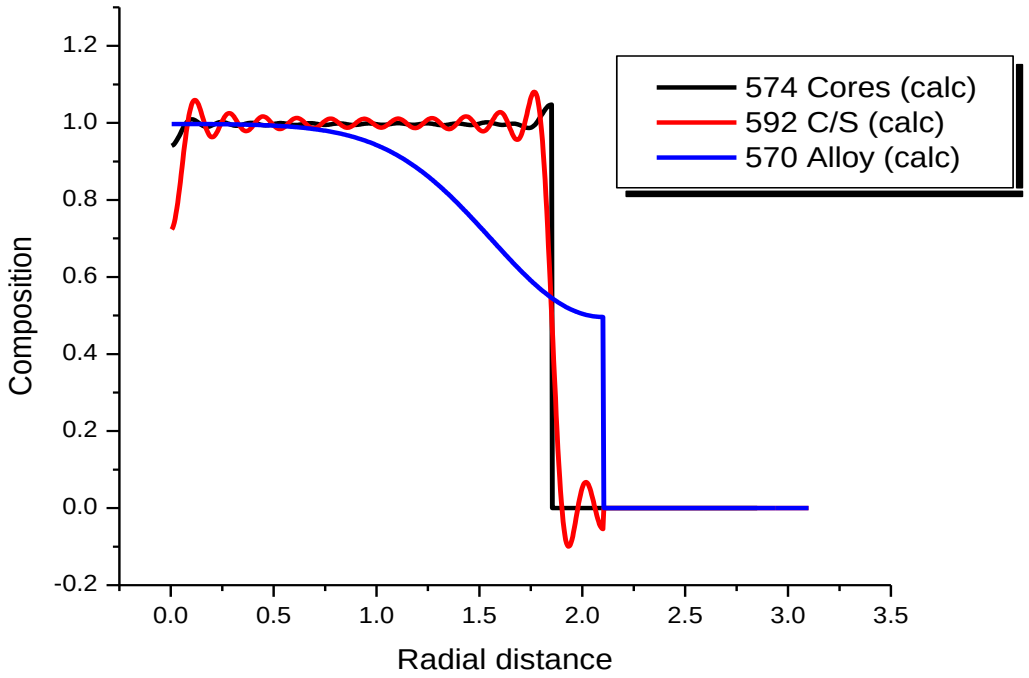

Figure 12: Radial composition profile for core, core/shell and core/shell alloy nanoparticles as calculated by the program described earlier.

The composition profiles in the above diagram show agreement with experimental observations in that the alloyed nanoparticles have the most uniform composition, and the core/shells have a flat composition curve corresponding to two separate regions, one of CdSe and one of ZnSe. After analyzing the interface between core and shell it is time to determine the auger rates from transient absorption experiments.

Transient Absorption Kinetics and Biexciton Auger Rates:

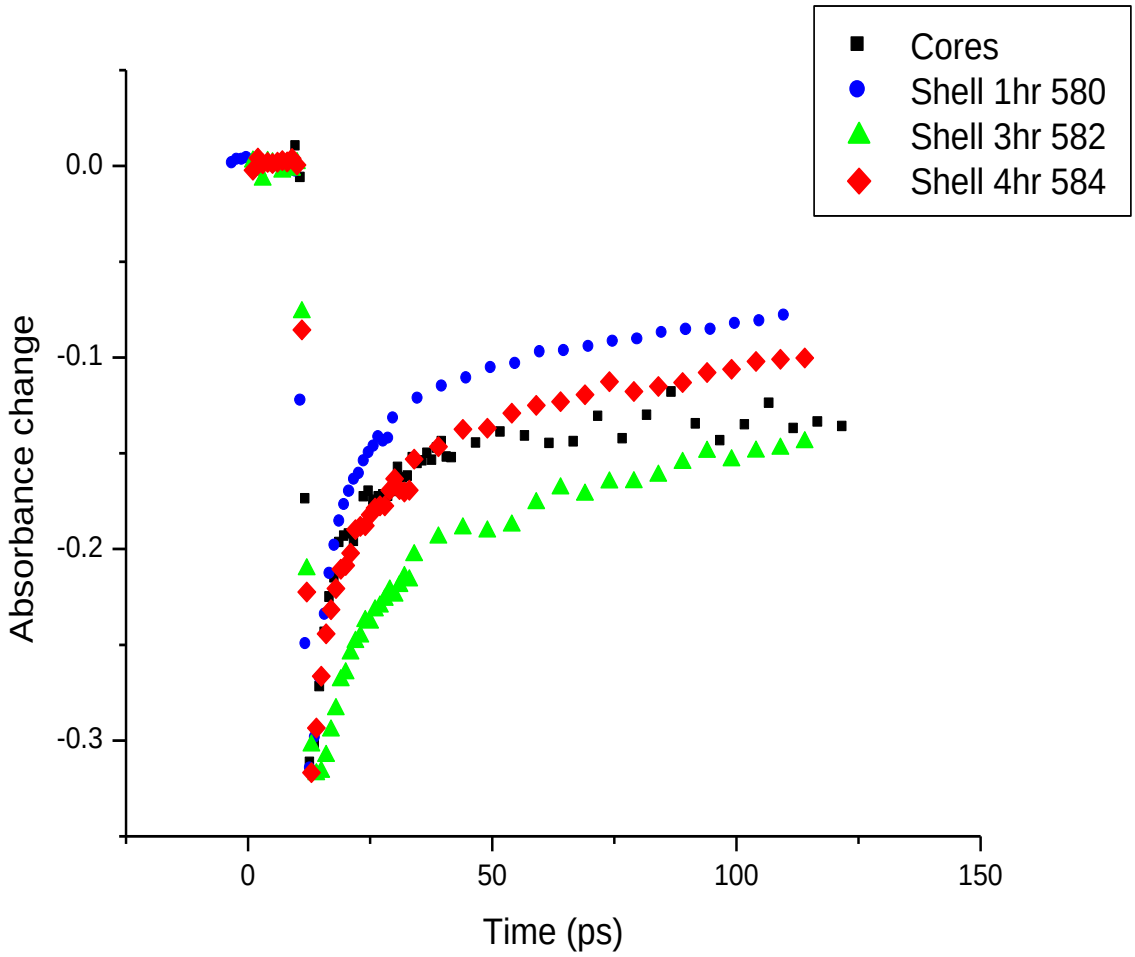

Figure 13: Transient absorption kinetics of CdSe cores and CdSe/ZnSe core/shells at various stages during the shelling process. Note the almost identical nature of the spectra despite the fact that the samples are very different from one another. For this experiment all samples had a concentration of $2x10^{14}$ particles/mL, and on average absorbed 5 photons each.

Transient absorption measures the absorbance of a sample over a very short time frame, in this case a few to a few hundred picoseconds. The samples were excited with 387nm light and the absorbance was measured every few picoseconds. Current theory suggests that the time it takes for multiexcitons to recombine (auger recombination) in a core/shell heterostructure

depends upon the sharpness of the interface between the two materials, and that alloying should increase the time it takes for this process to occur. The following figure analyzes the transient absorption kinetics for alloyed core/shell nanoparticles, and compared to the previous figure shows no apparent differences.

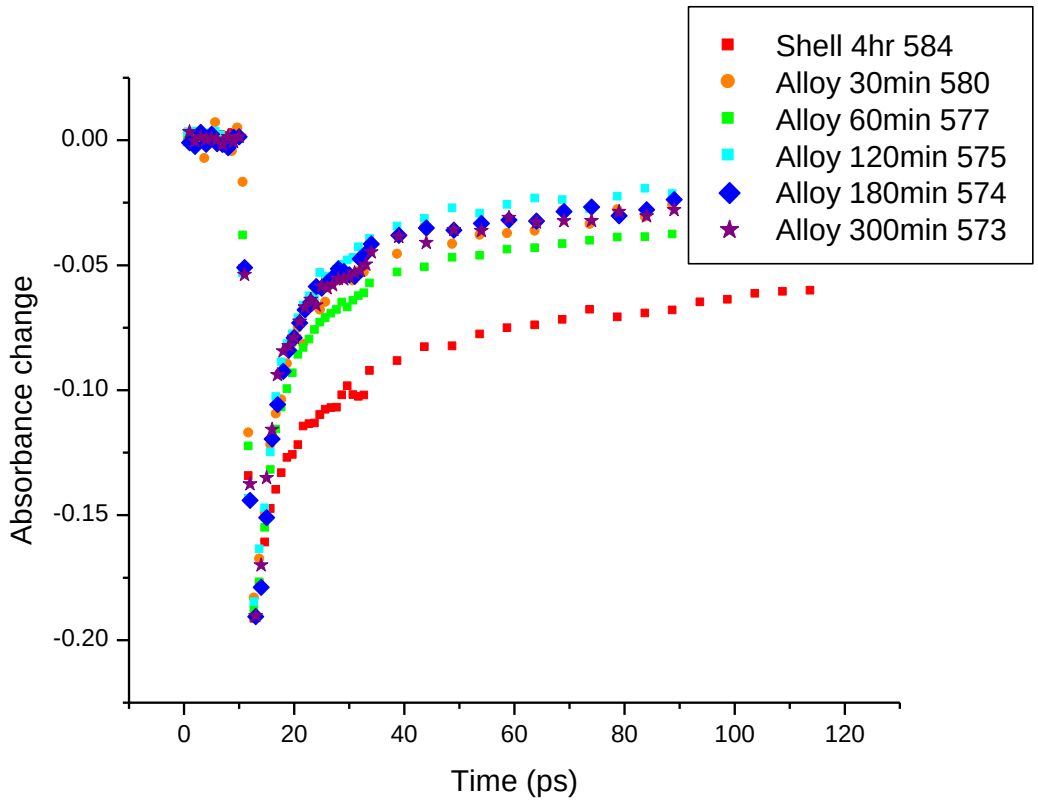

Figure 14: Transient absorption kinetics of alloyed CdSe/ZnSe core/shell nanoparticles. As the particles are alloyed for varying amounts of time the kinetic traces remain the same, so the decay kinetics did not change drastically when the composition of the core/shell particles was varied through annealing.

Because of the previously shown differences in the UV absorption, Raman and fluorescence of the alloyed particles compared to non-alloyed core/shell particles prepared in this experiment, it should come as a shock that the transient absorption kinetics are so similar. The experimental spectra do not support the conclusion that alloying core/shell nanoparticles changes

the absorption kinetics and auger rate. This result is contrary to what is found in the theoretical literature on this topic and is therefore an interesting result. Extracting the biexciton decay times by fitting the above curves to a biexponential (the rapid decay at early times is the biexciton decay time) function and plotting them together yields the following:

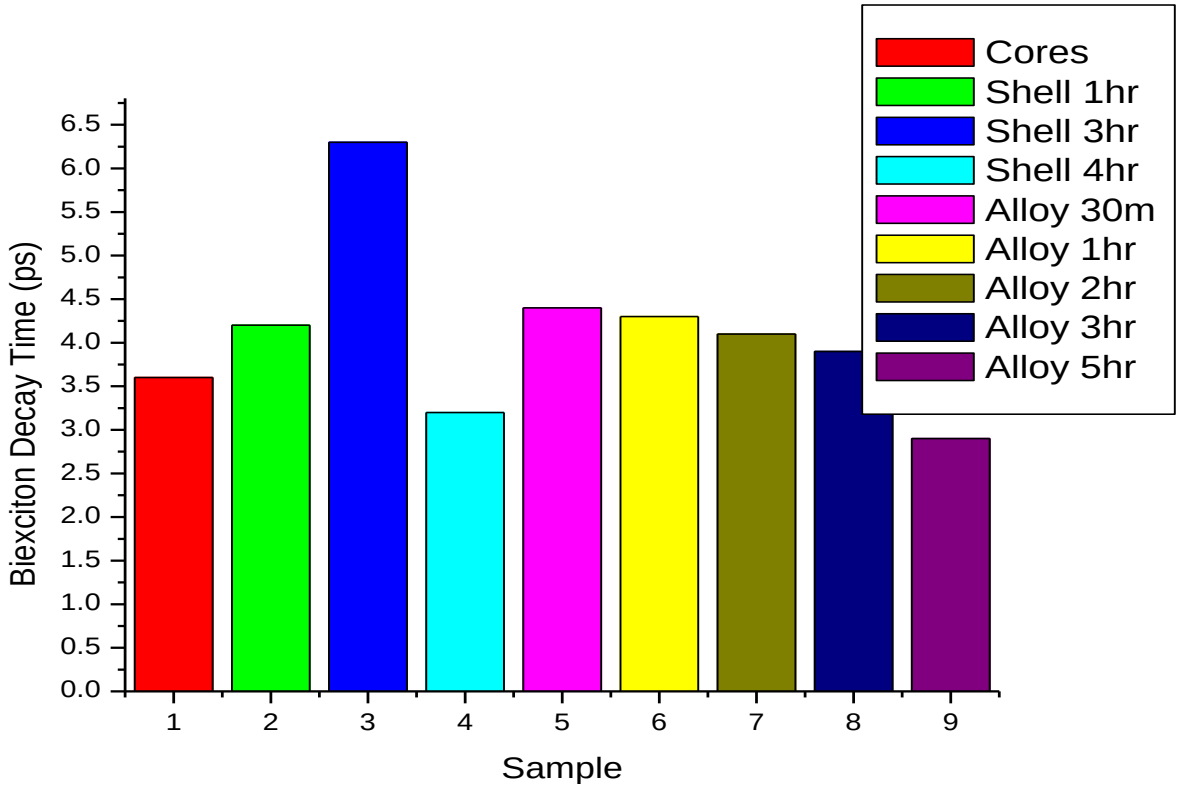

Figure 15: Biexciton decay times for nanoparticle samples from CdSe cores, to CdSe/ZnSe core/shells of various times during the shelling process, and finally CdSe/ZnSe core/shell alloys taken at various times during annealing at 250 degrees Celsius. These values are extracted from the transient absorption kinetics of figures 15 and 16, using the biexponential function $y = y_0 + A_1 e^{-x/t_1} + A_2 e^{-x/t_2}$. In this case t_1 are the biexciton decay times.

As can be seen from the above diagram, changing the composition of a core/shell nanoparticle by alloying does not have a drastic effect on the biexciton decay time which is a different result from published theoretical calculations [1]. Biexciton decay times are controlled by auger recombination, and support the conclusion that alloying does not change the rate of

auger recombination. The following plot of the single-exciton radiative decay times given below shows a similar result.

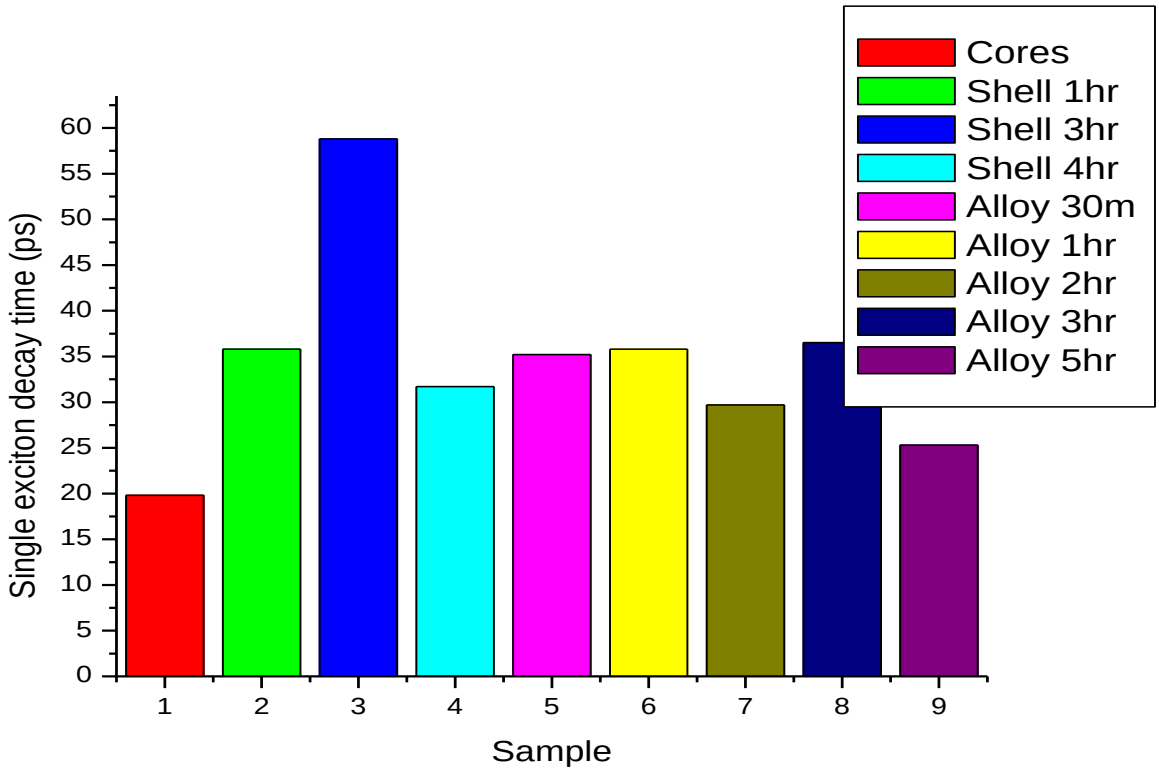

Figure 16: Single-exciton decay times for nanoparticle samples from CdSe cores, to CdSe/ZnSe core/shells of various times during the shelling process, and finally CdSe/ZnSe core/shell alloys taken at various times during annealing at 250 C. These values are extracted from the transient absorption kinetics of figures 15 and 16, using the biexponential function $y = y_0 + A_1 e^{-x/t_1} + A_2 e^{-x/t_2}$. In this case t_2 are the single exciton decay times.

It appears that alloying an interface between two materials has little to no effect on the biexciton auger rate or single exciton radiative decay rate, and therefore something else must be controlling them. One alternative explanation is that it is actually the surface of the particles, and the defects therein, that control these rates for core/shell nanoparticles. Also, defects in stacking of a shelling material on a core particle caused by lattice mismatch may have an impact on these rates. Take Shell 3hr from above as an example, it has both the longest single and biexciton

decay time, but once more shell adds on top of that defects are presumably created, lowering the decay time further. All of this makes sense if the rates are controlled by surface defects because changing the composition of the core/shell particles by alloying has little effect on either the single or biexciton decay times.

The final piece of information gathered from calculations was an estimation of the auger rate (recombination time of multiexcitons), and this was compared to the rate obtained from transient absorption experiments. Calculations showed only a slight difference in auger rates for the CdSe core, CdSe/ZnSe core/shell and CdZnSe alloy nanoparticles, a result that agrees with experimental spectra. This result is in direct contrast with existing theoretical predictions that stipulate alloying a core/shell interface should drastically reduce auger rates.

Conclusion

To conclude this work a few remarks on the experimental findings are in order. As was previously shown, alloying has no significant effect on the auger recombination dynamics of core/shell nanoparticles of CdSe/ZnSe, and this likely carries over to other semiconductor pairs as well. This conclusion is reinforced by the fact that single-exciton and multi-exciton decay rates followed the same pattern for all of the samples, and alloying all the samples for different amounts of time caused no changes in the dynamics. Current theory suggesting the abruptness of a potential energy function between two unlike materials as the reason for extremely rapid auger recombination processes is clearly not the case in the prepared particles. Other factors such as surface chemistry, defects in crystal lattices or redox scavengers in solution may be the primary contributors to this phenomenon, but more research on the topic is needed before definitive conclusions can be made.

References

[1] G.E. Cragg and A.L. Efros, "Suppression of Auger Processes in Confined Structures", *Nano Letters,* **10**, 313-317 (2010).

[2] J. van Embden, et al. "Review of the Synthetic Chemistry Involved in the Production of Core/Shell Semiconductor Nanocrystals", *Aust. J. Chem.*, **60**, 457-471 (2007).

[3] A.J. Nozik, "Multiple Exciton Generation in Semiconductor Quantum Dots", *Chemical Physics Letters*, **457**, 3-11 (2008).

[4] V. I. Klimov, "Mechanisms for Photogeneration and Recombination of Multiexcitons in Semiconductor nanocrystals: Implications for Lasing and Solar Energy Conversion", *J. Phys. Chem. B,* **110**, 16827-16845 (2006).

[5] X. Wang et al,"Non-Blinking Semiconductor Nanocrystals", *Nature Letters*, **459**, 686-689 (2009).

[6] R. D. Schaller et al, "Seven Excitons at a Cost of One: Redefining the Limits for Conversion Efficiency of Photons into Charge Carriers", *Nano Letters,* **Vol. 6, No. 3,** 424-429 (2006).

[7] M.D. Regulacio and Ming-Yong Han, "Composition-Tunable Alloyed Semiconductor Nanocrystals", *Accounts of Chemical Research,* **Vol. 43, No. 5**, 621-630 (2010).

[8] W. Shockley and H.J. Queisser, "Detailed Balance Limit of Efficiency of *p-n* Junction Solar Cells", *Journal of Applied Physics,* **Vol. 32, No. 3,** 510-519 (1961).

[9] J. J. Li et al. "Large-Scale Synthesis of Nearly Monodisperse CdSe/CdS Core/Shell Nanocrystals Using Air-Stable Reagents via Successive Ion Layer Adsorption and Reaction", *J. Am. Chem. Soc.*, **125**, 12567-12575 (2003).

[10] W. W. Lu et al. "Experimental Determination of the Extinction Coefficient of CdTe, CdSe, and CdS Nanocrystals", *Chem. Mater,* **15**, 2854-2860 (2003).

[11] V.D. Kleiman et al. "Synthesis and Characterization of Colloidal Ternary ZnCdSe Semiconductor Nanorods", *Journal of Chemical Physics,* **125**, 164711 (2006).

Appendix

Physical properties of relevant semiconductors[1]

Semiconductor	E_{cb}	E_{vb}	E_g	Density	V_m	A_0	C_0	mismatch
CdS (h)	4.1	6.6	2.52	4.82	29.92	.4135	.6749	-4, -4%
CdSe (h)	4.3	6.0	1.74(1.71)	5.82	32.9	.430	.702	0
CdTe (h)			1.44	6.2	38.7	.648		+5.6%
CdTe (c)	4.0	5.5	1.5	5.85	41.0			+7.6%
ZnS (c)	3.2	7.1	3.91	4.09	23.83	.541		-11.1%
ZnS (h)			(3.68)			.3811	.6234	
ZnSe (c)	3.5	6.2	2.58(2.82)	5.27	27.4	.567		-6.3% (5.668)
ZnSe (h)						.398	.693	
ZnTe (c)	3.6?	5.8?	2.24(2.39)	6.34	30.44		.610	+2.6%
ZnTe (h)						.427	.699	

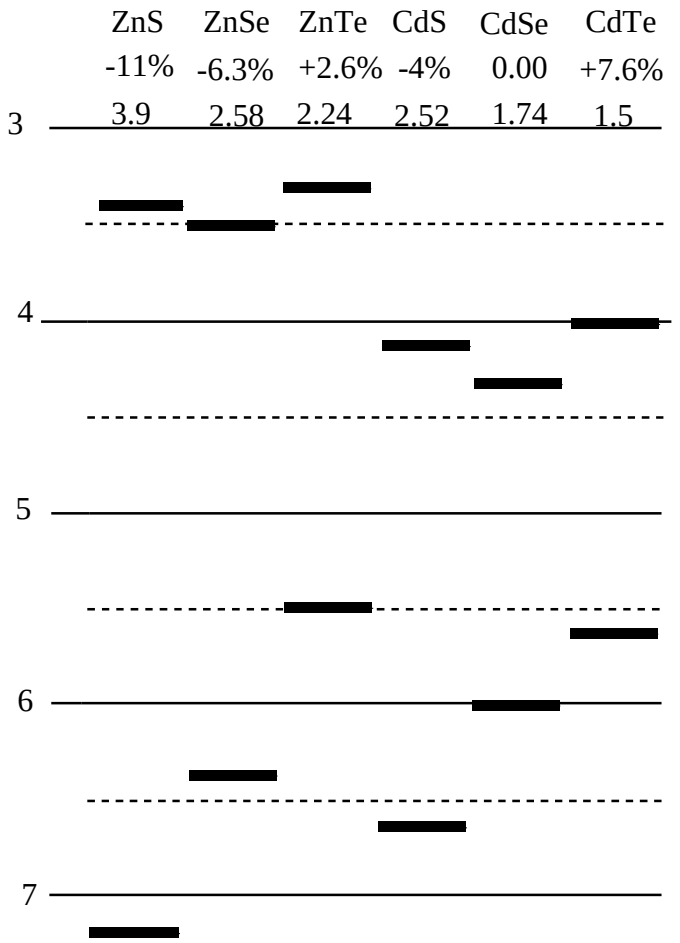

Type-I: CdSe/ZnSe, CdSe/CdS, CdTe/ZnSe,

Type-II: CdTe/CdSe, ZnTe/ZnSe, ZnTe/CdSe, ZnTe/ CdTe

ZnTe/CdSe (2.6%) and CdTe/ZnTe (4.8%) are very small lattice mismatches

CdSe bandgap is 1.74. Conduction band at about 4.3 V wrt vacuum, or at -0.2V vs. NHE. This puts hole at about 1.75V vs. NHE. Effective masses are 0.11 (electron) and 0.44 (hole).[2]

Lattice parameters are at http://www.semiconductors.co.uk/propiivi5410.htm#CdS,CdSe,CdTe

More generally, at http://www.semiconductors.co.uk/propiivi5410.htm

The reference is D W Palmer, www.semiconductors.co.uk, 2008.03. *The data for the lattice parameters are quoted from A R West "Basic Solid State Chemistry" (Wiley 1988), which states them to be from R W G Wykoff, "Crystal Structures" (Wiley 1971) Vol 1.(other values for band gaps in parentheses)*

1. Embden, J. v.; Jasieniak, J.; Gomez, D. E.; Mulvaney, P.; Giersig, M., Review of the Synthetic Chemistry in the Production of Core/Shell Semiconductor Nanocrystals. *Aust. J. Chem.* **2007,** 60, 457.

2. Rogach, A. L.; Kornowski, A.; Gao, M.; Eychmuller, A.; Weller, H., Synthesis and Characterization of a Size Series of Extremely Small Thiol-Stabilized CdSe Nanocrystals. *J. Phys. Chem. B* **1999,** 103, 3065.

3. Cook, A. R.; Curtis, L. A.; Miller, J. R., Fluorescence of the 1,4 benzoquinone radical anion. *J. Am. Chem. Soc.* **1997,** 119, 5729.

4. Burda, C.; Green, T. C.; Link, S.; El-Sayed, M. A., Electron shuttling across the interface of CdSe nanoparticles monitored by femtosecond laser spectroscopy. *J. Phys. Chem. B* **1999,** 103, 1783.

5. Logunov, S.; Green, T.; Marguet, S.; El-Sayed, M. A., Interfacial carrier Dynamics of CdS nanoparticles. *J. Phys. Chem. A* **1998,** 102, 5652.